Astron. Astrophys. 327, 513–521 (1997)

ASTRONOMY AND ASTROPHYSICS

The high-frequency compact radio structure of the peculiar quasar 4C 39.25

A. Alberdi[1,2], T.P. Krichbaum[3], D.A. Graham[3], A. Greve[4], M. Grewing[4], J.M. Marcaide[5], A. Witzel[3], R.S. Booth[6], L.B. Bååth[6], F. Colomer[6,7], S. Doeleman[8], A.P. Marscher[9], A.E.E. Rogers[8], C.J. Schalinski[4,10], and K. Standke[3]

[1] Laboratorio de Astrofísica Espacial y Física Fundamental, Apdo. 50727, E-28080 Madrid, Spain
[2] Instituto de Astrofísica de Andalucía, CSIC, Apdo. 3004, Granada, Spain
[3] Max Planck Institut für Radioastronomie, Auf dem Hügel 69, D-53121 Bonn, Germany
[4] IRAM, Domaine Universitaire, Grenoble, France
[5] Departamento de Astronomía, Universitat de València, E-46100 Burjassot, Spain
[6] Onsala Space Observatory, Onsala, Sweden
[7] Observatorio de Yebes, Apdo. 148, Guadalajara, Spain
[8] NEROC, Haystack Observatory, Westford, Massachusetts, USA
[9] Boston University, Boston, MA, USA
[10] now at Institut für Weltraumsensorik (DLR), Rudower Chaussee 5, D-12489 Berlin, Germany

Received 24 February 1997 / Accepted 2 April 1997

Abstract. We present new high angular resolution images of the compact non-thermal radio source 4C 39.25 obtained from VLBI observations at λ1.3 cm, λ7 mm, and λ3 mm wavelengths. These maps and Gaussian modelfits show that the milliarcsecond to sub-milliarcsecond structure of 4C 39.25 consists of a complex bent core-jet structure with embedded moving and stationary VLBI components. Facilitated by the small observing beams and high angular resolutions obtained at mm-wavelengths, we measured the relative positions of the jet components with an accuracy of a few hundred micro-arcseconds. This allows the detailed followup of the ongoing merging process of a westward superluminally moving component (b) with a stationary component a, located at ∼2.9 mas east of the putative core d. In contrast to the other components of the structure with steeper spectra, the westernmost component d exhibits an inverted spectrum peaking between λ7 mm and λ3 mm, thus further supporting its identification as the VLBI core, self-absorbed at longer wavelengths.

From two VLBI maps obtained nearly simultaneously at λ7 mm and λ1.3 cm, we made the first spectral index map of 4C 39.25 in this wavelength regime. The main characteristics of the spectral index distribution of the jet are pronounced changes of the spectral index between orientations parallel and transverse to the jet axis. Near the merging components a and b the spectral index steepens with increasing separation from d. However, in the bridge of emission c, which connects d with a and b, the spectral index gradient has a direction transverse to the jet axis, suggesting a frequency dependent jet curvature and edge-brightening. A brief discussion of this behaviour within current jet models is presented.

Key words: galaxies: jets – quasars: 4C 39.25 – techniques: interferometric – radio continuum: general

1. Introduction

During the last 10 years, several groups have performed VLBI observations of the peculiar superluminal radio source 4C 39.25 at wavelengths λ=1.3, 2.8 and 3.6cm (Marcaide et al. 1985; Shaffer et al. 1987; Marscher et al. 1987; Marcaide et al. 1989; Marcaide et al. 1990; Zhang et al. 1990; Marscher et al. 1991; Alberdi et al. 1993a, 1993b; Marcaide et al. 1994). These observations have revealed the presence of a superluminal component (b) moving between the western components (c and d) and the eastern component (a). Components a and c have remained stationary relative to each other and constant in flux density, while component b has brightened and its motion slowed down as it approached component a (Alberdi et al. 1993a). Recent VLBI observations at λ7mm and 1.3cm suggested that the westmost component d, with a weak and inverted spectrum and located ∼2.7±0.2 mas west of a, could be the core of 4C 39.25 (Alberdi et al. 1993b).

The parsec scale radio structure of the radio source 4C 39.25 has been interpreted in the framework of the relativistic jet model (e.g. Blandford & Königl, 1979) adding jet curvatures to explain the coexistence of moving and stationary components

Send offprint requests to: A. Alberdi

(Marcaide et al. 1989, 1990, Marscher et al. 1991, Alberdi et al. 1993a, Marcaide et al. 1994). In this model, i) component d would be interpreted as the synchrotron-self-absorbed "VLBI-core" of the jet of 4C 39.25; ii) the apparent stationarity of the components a and c would be explained by the presence of bends in the jet trajectory (Alberdi et al. 1993b); iii) the motion and flux density evolution of b would be explained by the emission from a shock wave travelling along a bent relativistic jet. According to this model, the mas-structure of 4C 39.25 would be determined by emission from the quiescent flow of the underlying jet, by emission from shocks and by the geometrical orientation of the emitting regions relative to the observer's line of sight.

Global VLBI observations performed in 1990.5 at 7mm provided a first map of 4C 39.25 at this wavelength (Alberdi et al. 1993b). At that time, however, the quality of the 7 mm maps was limited by the small number of participating VLBI antennas and the resulting poor uv-coverage. In this paper we now present new results from higher quality 7mm VLBI-observations of 4C 39.25 performed in 1992.4. The addition of four VLBA antennas[1] and the 30 m MRT at Pico Veleta (Krichbaum et al. 1993a) to the preexisting 7mm-array (see e.g., Bartel et al. 1988; Krichbaum et al. 1992 & 1993a) has considerably improved the imaging capabilities, leading to the first high dynamic range image of 4C 39.25 at λ7 mm, which we present here.

Shortly after the 7mm VLBI experiment, global VLBI observations of 4C 39.25 were made at 1.3cm using 14 stations (epoch 1992.44), which resulted in a VLBI map with a dynamic range (300:1) comparable to that of the 7mm map (200:1).

Additionally, the analysis of snapshot-type data from a 3mm VLBI experiment performed in 1993.26 (Standke et al. 1994) yielded at this wavelength a Gaussian model for 4C 39.25 which reflects quite well the basic source structure seen at longer wavelengths and also confirms the existence and the inverted spectrum of component d.

For 4C 39.25, the high angular resolution of mm-VLBI observations provides an unique opportunity to study and further follow the merging process of b and a, up to relative separations an order of magnitude below the angular resolution provided by VLBI observations at cm-wavelengths. Together with complementing kinematic and spectral information obtained at these longer wavelengths, our understanding of the physical processes acting in the bent jet of 4C 39.25 can be improved.

2. Observations and data reduction

2.1. Observations at λ1.35cm

4C 39.25 was observed at λ1.35 cm for 14 hours on June 11, 1992 with a global VLBI network consisting of 14 stations (see Table 1). Recording was done using the MKII VLBI system (Clark et al. 1973), with a 2 MHz band centered at a frequency of 22228.99 MHz. The data were correlated at the Block2 correlator at the California Institute of Technology. After correlation the data were reduced in the standard manner (for details see e.g. Alberdi et al. 1993a), including fringe-fitting, segmentation into 60 seconds intervals (to avoid coherence losses larger than 10%), calibration, data editing and final image reconstruction. Table 1 summarizes the average system temperatures and nominal gains during the observations.

Table 1. Antenna characteristics at 1.3 cm

Station	Code	D $[m]$	T_{sys} $[K]$	Gain K/Jy	Pol.
Effelsberg	B	100	140	0.790	LCP
Onsala	S	20	320	0.056	LCP
Medicina	L	32	150	0.110	LCP
Metsahovi	V	14	50	0.027	LCP
Haystack, MA	K	37	120	0.135	LCP
Green Bank	G	43	100	0.061	LCP
Los Alamos, NM	LA	25	105	0.103	LCP
Pie Town, NM	PT	25	100	0.128	LCP
Kitt Peak, AZ	KP	25	103	0.114	LCP
North Liberty, IO	NL	25	116	0.097	LCP
Fort Davis, TX	FD	25	90	0.094	LCP
Brewster, BR	BR	25	120	0.098	LCP
Owens Valley, CA	OV	25	100	0.077	LCP
Phased-VLA, NM	Y	–	110	1.000	LCP

2.2. Observations at λ7mm

The observations at λ7 mm were performed as part of a larger global 7mm-VLBI observing campaign in which, besides 4C 39.25, other active galactic nuclei were observed (Krichbaum et al., 1993c, 1994, 1995). 4C 39.25 was observed on May 26th, 1992, from 13h45 UT for 14 hrs with 8 stations. Table 2 summarizes the characteristics of the participating antennas. The data were recorded using the Mk III VLBI system (Rogers et al. 1983) in mode B, double speed (bandwidth 56 MHz). The observations were made at a center frequency of 43220.99 MHz and intended to be made with left circularly polarized feeds. However, due to problems in the definition of the polarization of the receiver feeds, the antennas at the VLBA and at Pico Veleta recorded RCP, while the antennas Effelsberg, Haystack and Onsala recorded LCP. The data were correlated at the MK III correlator of the MPIfR at Bonn. To avoid problems with cross polarization on the mapping procedures, only the baselines with parallel handed polarization were correlated. Thus, two subsets of data (3 baselines in LCP; 10 baselines in RCP) were obtained, which after consistency checks were finally combined. uv-coverages for the observations at 7 mm and 1.35 cm are shown in Fig. 1.

2.3. Observations at λ3mm

The observations at λ3mm were made on April 6th, 1993. These observations were also part of a larger global observing cam-

[1] The VLBA is operated by Associated Universities Inc. under cooperative agreement with the US National Foundation

Table 2. Antenna characteristics at 7 mm

Station	Code	D $[m]$	T_{sys} $[K]$	Gain K/Jy	Pol.
Effelsberg	B	60[1]	390	0.296	LCP
Onsala	S	20	450	0.055	LCP
Haystack, MA	K	37	280	0.060	LCP
Pico Veleta	PV	30	250	0.180	RCP
Los Alamos, NM	LA	25	110	0.097	RCP
Pie Town, NM	PT	25	110	0.098	RCP
Kitt Peak, AZ	KP	25	136	0.096	RCP
North Liberty, IO	NL	25	113	0.079	RCP

[1]Note: For Effelsberg, the diameter of the illuminated surface is given.

Table 3. Antenna characteristics at λ3mm

Station	Code	D $[m]$	T_{sys} $[K]$	Gain K/Jy	Pol.
Effelsberg	B	60[1]	400	0.130	LCP
Onsala	S	20	400	0.056	LCP
Pico Veleta	PV	30	200	0.140	LCP
Haystack	K	37	250	0.058	LCP

[1]Note: For Effelsberg, the diameter of the illuminated surface is given.

paign. The data were recorded with the Mk III equipment, in mode A at double speed (bandwidth 112 MHz). The main aim of this 3mm-VLBI campaign was the experimental verification of the expected theoretical detection sensitivity for VLBI observations at 86 GHz and the detection of source candidates suitable for future studies. Four sensitive antennas – characteristics shown in Table 3 – observed about 20 compact radio sources in snapshot mode at the center frequency 86.241 GHz. Further observational details and results on the detection limits are given in Standke et al. (1994) and Krichbaum et al. (1994). 4C 39.25 was detected in several scans (each of 6.5 min duration) on all baselines to Pico Veleta with signal-to-noise ratios in the range of 7 to 14 and on the baseline Effelsberg-Onsala with signal-to-noise ratios in the range of 9 to 10.

2.4. Fringe fitting and calibration

At 7 mm and 3 mm wavelengths, the initial fringe searches were made independently for each baseline with wide search windows for fringe-rate, single and multi-band delay, using the standard software provided for the MK III VLBI system (Rogers et al. 1983). In a second refringing phase and in order to further enhance the detection probability, we iteratively lowered the widths of the fringe search windows using the global fringe fitting algorithm based on closure relations (Alef & Porcas, 1986) and estimates of the a priori single- and multi-band delays from adjacent detections of 4C 39.25 and of other bright sources observed shortly before and after 4C 39.25. With this procedure it was possible to lower the detection threshold to $SNR \simeq 5$ for those scans for which closure-triangles could be constructed (Krichbaum et al. 1992). After fringe-fitting, the data were segmented into time intervals of 20 sec (at 7mm) and of 10 sec (at 3mm) to avoid coherence losses larger than 10%.

The data were then exported into the Caltech VLBI package (Pearson 1991), where editing and amplitude calibration were done with similar procedures for the three frequencies. Starting from the initial calibration provided by the observatories (a priori system- and antenna-temperature measurements, elevation dependent antenna gain curves), we corrected the VLBI data for atmospheric opacity effects (eg. Krichbaum et al. 1993b). For some of the stations, and mainly at the higher frequencies, time-variable opacity corrections were required to correct for changing weather conditions during the observations. The accuracy of the overall amplitude calibration was judged by comparing the relative antenna gain corrections obtained independently from the standard self-calibration method on calibrator and program sources, and from the atmospheric opacity-corrections, when combined with the nominal gain curves. On this basis, we can confidently assign uncertainties in the amplitude calibration of 5-10 % at 22 GHz, $\sim$ 10 % at 43 GHz, and $\sim$ 20-30 % at 86 GHz. At 86 GHz not very accurately known antenna aperture efficiencies and peak-values of the gain curves may cause shifts of the absolute flux density scale.

3. Modelling and imaging results

The brightness distributions of 4C 39.25 at 22 GHz and 43 GHz were derived from iterative procedures of modelfitting, hybrid-mapping (Cornwell & Wilkinson 1981) and moderate changes of the amplitude calibration. The final maps were obtained using the difference mapping procedure (DIFMAP, Pearson et al. 1994). The parameters of the structure components were obtained from fits of elliptical Gaussian components to the final self-calibrated visibility data (see Table 4). Our analysis of the 86 GHz data was based on model fitting only, due to the limited amount of data, the sparse uv-coverage and the low signal-to-noise ratios of the detections.

In Fig. 2 we show the CLEAN-maps of 4C 39.25 at 22 GHz and 43 GHz. Both maps have a comparable dynamic range, with the lowest significant contour level at about 0.3-0.5 % of the peak flux density. In order to compare the source structures at the 3 different frequencies, we convolved the above two maps and the Gaussian model obtained from the 3 mm data with a beam of size 0.60×0.30 mas , oriented at P.A. 12° . Fig. 3 summarizes the result. Table 4 lists the results from the model fitting.

4. Discussion

The comparison of the maps shown in Fig. 2 and Fig. 3 with each other and with maps obtained earlier at wavelengths longer than λ = 1.3 cm (Alberdi et al. 1993a, Marcaide et al. 1994) and at λ = 7 mm (Alberdi et al., 1993b), leads to a component identification indicated by labels in Table 4: starting from the westernmost component d with inverted spectrum (see below), a faint and partially bent bridge of 2-3 sub-components of the component c connects d with the brightest jet component, la-

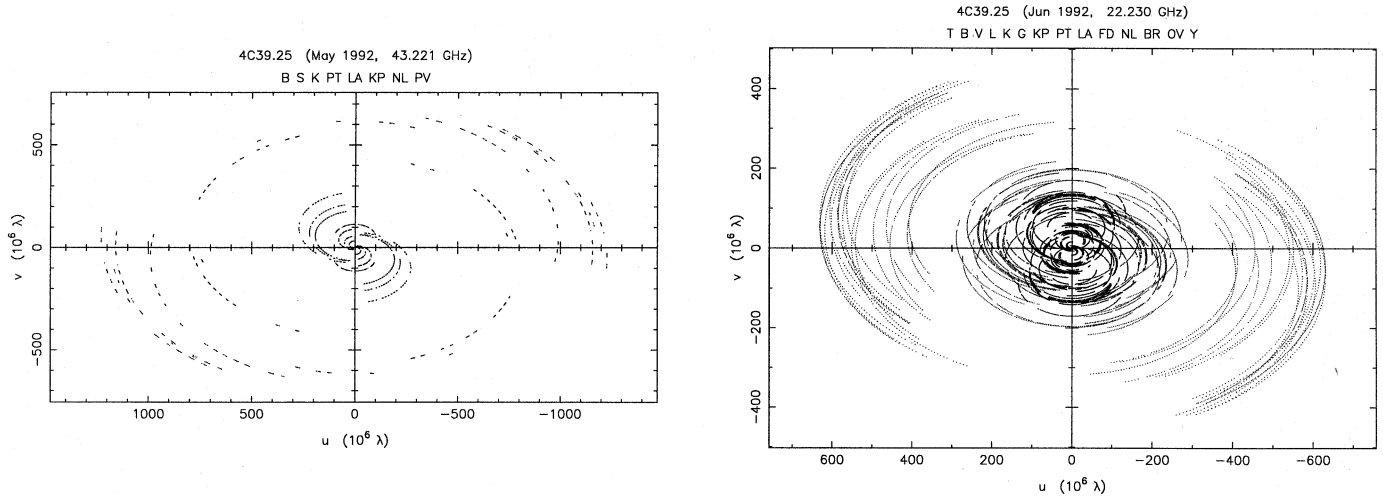

Fig. 1. uv-coverages for the observations of 4C 39.25 at 7 mm and 1.35 cm (left and right, respectively).

Table 4. Parameters of Gaussian model-fit components for 4C 39.25[1]

Component identification	Flux Density (Jy)	Radius[2] (mas)	Theta[3] (deg)	Axis[4] (mas)	Ratio[5]	Phi[6] (deg)
Model at λ1.3cm	11 June 1992					
a	1.32±0.04	0.40±0.01	92±4	0.21±0.10	0.85±0.05	54±15
b	6.42±0.05	0.0	0	0.36±0.05	0.91±0.05	23±10
c1	0.09±0.02	0.52±0.20	325±30	0.42±0.25	0.30±0.10	48±15
c2	0.30±0.05	1.21±0.45	292±10	0.79±0.30	0.30±0.10	81±10
c3	0.21±0.15	1.95±0.05	283±3	0.40±0.05	0.30±0.10	–71±10
d	0.20±0.02	2.48±0.02	283±2	0.10	0.30	96±5
Model at λ7mm	26 May 1992					
a	0.41±0.05	0.41±0.02	86±5	0.37±0.15	0.29±0.10	137±10
b	3.47±0.03	0.0	0	0.33±0.05	0.93±0.10	81±10
c1	0.05±0.02	0.53±0.20	326±10	0.39±0.25	0.30±0.10	70±15
c2	0.10±0.05	1.28±0.26	299±5	0.76±0.60	0.30±0.10	106±10
c3	0.11±0.02	1.97±0.07	288±3	0.27±0.14	0.30±0.10	–45±10
d	0.29±0.02	2.48±0.02	283±2	0.10	0.30	140±12
Model at λ3mm	6 April 1993					
a	0.57±0.20	0.36±0.10	111±20	0.15±0.10	0.30±0.10	–40±20
b	2.05±0.30	0.0	0	0.33±0.10	0.28±0.10	2±15
d	0.20±0.10	2.55±0.20	279±10	0.10	0.10	37±15

Notes: [1]Parameters without error bars were kept fixed in the least-squares solution. [2]Relative separation with respect to component b. [3]Position angle with respect to component b. [4]Major axis of the elliptical Gaussian. [5]Ratio between the minor and major axis. [6]Orientation of the major axis.

belled b. We have used in the maps and models of Fig. 3 and Table 4 component b as reference point. The relative distance between d and b at epoch 1991.5 is $r \sim 2.5$ mas. At the same epoch, component a is located $r \sim 0.4$ mas east of b, and thus the overall source extension is ~ 2.9 mas.

4.1. Motion of d

The distance between a and d has not changed significantly within a period of 6 years, since the time in which component d was detected (Marcaide et al. 1990; Alberdi et al. 1993a, 1993b). This leads to an upper limit for the proper motion μ of component d of 0.03 mas yr^{-1}, corresponding to $\beta_{app} \leq 0.65h^{-1}$ (for H_o = 100h $km\ s^{-1}\ Mpc^{-1}$, q_0=0.5).

4.2. A bridge of emission

Mainly due to the improved dynamic range of the images at 1.3cm and 7mm, we were able to detect several fainter jet components, some of them previously unseen. These features seem to form a slightly bent 'bridge of emission' connecting d and b. Although this 'bridge' appears as a continuous brightness dis-

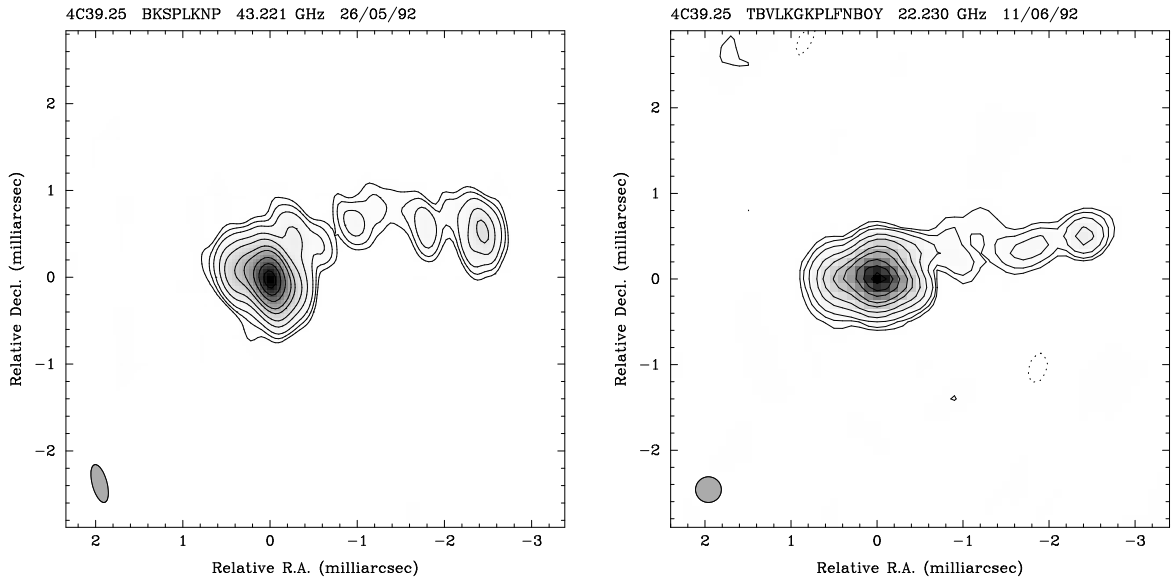

Fig. 2. VLBI images of 4C 39.25 at 7 mm and 1.3 cm wavelength (left and right, respectively). The 7 mm map is displayed with a restoring beam size of 0.45×0.17 mas oriented at position angle 15 deg. The contour levels are -0.5, 0.5, 1, 2, 5, 10, 20, 30, 50, 70 and 90% of the peak brightness of 1.46 Jy/beam. The 1.3 cm map is displayed with a restoring beam size of 0.30×0.30 mas. The contour levels are -0.5, 0.5, 1, 2, 5, 10, 20, 30, 50, 70 and 90% of the peak brightness of 3.03 Jy/beam.

tribution, we attempted to parametrize it by discrete Gaussian components. Best results were obtained with 3 Gaussian components located at r$\sim$ 0.53 mas, r$\sim$ 1.28 mas, and r$\sim$ 1.96 mas with respect to b and which we have labelled as c1, c2, and c3. The comparison of the position angles of the 3 components seen at 1.3 cm and 7 mm indicates a frequency dependent structure and curvature of the bridge. This is also clearly visible in the maps (see Figs. 2 and 3).

Previous maps obtained at longer wavelengths with lower resolution showed the presence of a component located at about 2 mas west of a, respectively 0.8 mas east of d, which was labeled c. Due to its steep spectrum (spectral index of c: $\alpha_{8.4/10.7\,GHz} = -0.98$, with α defined by $S \propto \nu^{\alpha}$) and the higher resolution at 22 GHz, respectively 43 GHz, component c appears fainter and seems to break up into the two subcomponents c2 and c3, while component c1 was not visible before at lower resolutions. The region associated with the bridge seems to be partially resolved by the interferometer beam and perhaps its emission is related to emission of the underlying quiescent relativistic flow, connecting d with a. The future detection of motion in this bridge, if any, should give constraints to the velocity (Lorentz factor) and orientation (inclination angle) of this region, which then could be compared with the corresponding numbers resulting from the motion of b.

4.3. Deceleration and brightening of b

In Fig. 4 we plot the decreasing separation of b with respect to a as a function of time, r(t). Data points prior to 1992 have been taken from the literature. The new data points from this paper confirm that the motion of b is not uniform. A least-squares fit to the data formally yields apparent deceleration of the motion of b parametrized as follows: $r(t) = a_2(t-t_0)^2 + a_1(t-t_0) + a_0$, with $a_0 = 2.05 \pm 0.05$ mas, $a_1 = -0.258 \pm 0.020$ mas/yr and $a_2 = 0.010 \pm 0.002$ mas/yr^{-2}, where t is measured in years and t_0 is the back-extrapolated time of the appearance of b in t_0 = 1980.3 (Alberdi et al. 1993b). This corresponds to an apparent decrease of the superluminal speed from β = 3.6 in 1989 to β = 2.1 in 1992.5.

While component b is approaching a (the high angular resolution of future mm-VLBI observations is required to further follow this encounter) its flux density is brightening considerably: between September 1989 and June 1992 the total 22 GHz flux density of 4C 39.25 increased from 5.1 Jy to 8.7 Jy. In the same time interval the flux density of b increased by basically the same amount (from 2.6 Jy to 6.4 Jy). This strong correlation and the fact that the high frequency spectrum of b is flattening progressively between 1990 and 1992, strongly supports the model of a geometrical cause for the correlated brightening and deceleration of b as earlier pointed out. Motion of b along a bent path with curvature towards the observer's line of sight can easily explain the observed behaviour.

4.4. Spectral characteristics and a spectral index map

From the two quasi-simultaneous VLBI maps made at 1.3 cm and 7 mm it is possible to derive a spectral index map.

The detailed shape of a spectral index map, however, critically depends on the way in which both maps are super-imposed. For models of synchrotron-selfabsorbed jet components their relative separation (and absolute position with respect to a fiducial reference point) depend on frequency and opacity (Bland-

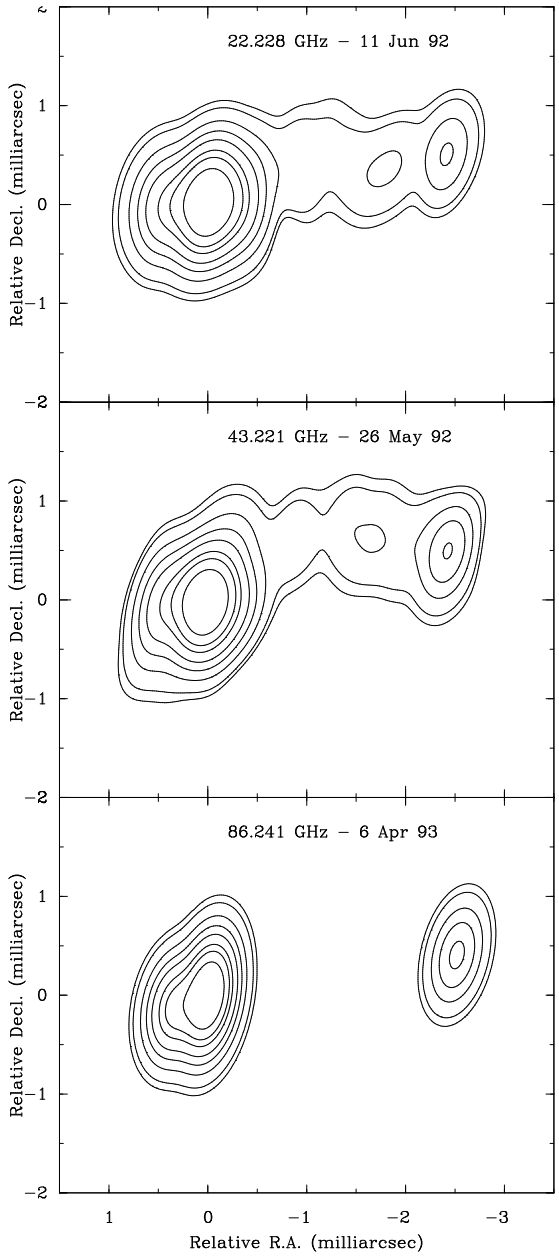

Fig. 3. VLBI images based on CLEAN-maps of 4C 39.25 at 1.3 cm and 7 mm and a Gaussian model fit at 3 mm. The maps are displayed with a common restoring beam size of 0.60×0.30 mas, PA=12° . The contour levels are 0.5, 1, 2, 5, 10, 20, 30, 50, 70 and 90% of the peak brightness of 3.84 Jy/beam, 2.15 Jy/beam and 1.71 Jy/beam, respectively.

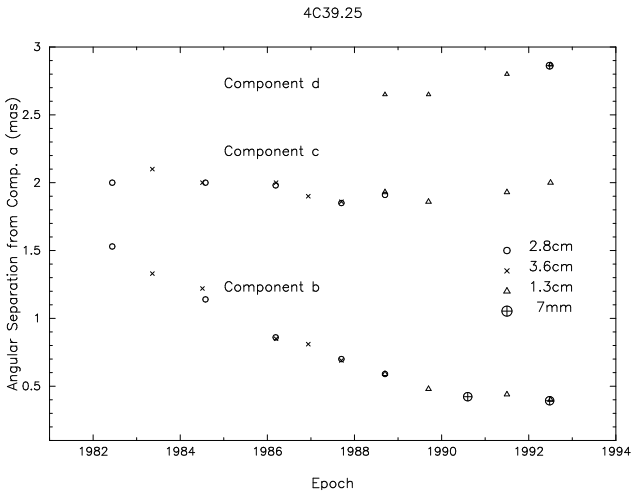

Fig. 4. Angular separation (in [mas]) of the components b, c and d with respect to component a plotted versus time (in [yrs]). Data prior to 1992.50 are from observations at 2.8 & 3.6 cm: Shaffer et al. , 1987 (and references therein); 3.6 cm: Marscher et al. , 1987 (and references therein); 1.3, 2.8 and 3.6 cm: Alberdi et al. , 1993a; 7 mm: Alberdi et al. , 1993b.

ford & Königl, 1979; Gómez et al. 1993, 1994; Alberdi et al. 1993c). Frequency dependent position shifts of VLBI components are observed in a number of sources, eg.: with S/X-band phase referencing VLBI a 0.7 mas-shift of the core position of 1038+528 A was found with respect to the external reference source 1038+528 B (Marcaide & Shapiro, 1983). In 3C 345 frequency dependent shifts of the relative core separations of the moving jet components of $\Delta r_{22/10.7\,GHz} \simeq 0.2 - 0.3$ mas are reported by Biretta et al. (1989) and Lobanov (1995).

To estimate effects related to an incorrect alignment of both maps caused by opacity effects and/or resulting from the differences in the uv-coverage of both data sets, we have made several spectral index maps using the maps shown in Fig. 2 and Fig. 3. Keeping arbitrarily the 1.3cm image fixed, we shifted (in α and δ) the 7mm image with respect to the 1.3cm image. Additionally, we varied the x-y gridding used for the reconstruction of spectral index map, and we convolved both maps with different beam sizes.

For relative displacements larger than 0.1 mas in right ascension, we obtain spectral index distributions with spectral indices rapidly oscillating along the jet between steep and inverted values. Such extreme spectral index variations seem to us quite unrealistic (both, transversal and longitudinal spectral index gradients are distributed along the jet quite arbitrarily, therefore of little reliability).

On the basis of the maps and modelfits we found that the relative position of b with respect to d (and vice versa) is basically the same at 22 and 43 GHz, with no evidence for any east-west displacement between 22 and 43 GHz of d with respect to b. Thus both maps could be centered on the connecting line between b and d, which required no shifts if for example both maps are initially centered on b. The spectral index map shown in Fig. 5 was made this way, after gridding the 22 & 43 GHz images to an identical x-y grid and convolving it with a common beam of 0.6 × 0.3 mas, oriented along P.A.= 12° . The basic characteristics of the spectral index distribution of 4C 39.25 can be summarized as follows:

(i) it shows an inverted spectrum region associated with component d,
(ii) with increasing separation from d, the spectral index seems

to get steeper,
(iii) it shows complex spectral index variations with spectral gradients along *and* perpendicular to the mean jet axis.

In the following we discuss items (i), (ii), and (iii).

(i)Component d has an inverted spectrum while all the other components exhibit relatively steep spectra. From the modelfits, we obtain an inverted spectral index for d between 22 and 43 GHz of α_d = +0.6 ($S \propto \nu^{\alpha}$), consistent with the spectral index distribution in Fig. 5. The 7mm & 3mm data suggest a spectral turnover of d in the range $43 \leq \nu_{max} \leq 86$ GHz. This and the high compactness of d suggests that d is the self-absorbed core of the radio source. Such interpretation is also supported from the observed stationarity of d with respect to a, given that a has been found to be stationary with respect to an external compact extragalactic reference source (0920+390), located 0.75° appart (Guirado et al. 1995).

For most AGN observed so far with VLBI, the flux density of the VLBI cores is quite variable. The low degree of flux density variability of d, however, brings some doubts on its identification as VLBI core (i.e. the selfabsorbed base of the jet). We therefore cannot rule out that d might be another self-absorbed jet component, in the vicinity of the still invisible real core of the source. The present lack of apparent motion could then be explained by another twist of the jet-axis, similar to the one used to interpret the stationarity of a and c (Alberdi et al. 1993a). The detection of apparent motion and/or spectral ageing of d would be a critical test to reveal the true nature of d. In any case, the lack of proper motion for d will leave always the question not definitely resolved.

(ii) As mentioned before, the components a, b and c exhibit steep spectra. In particular, the spectral index between 22 and 43 GHz for a is $\alpha_a = -1.8$ and for b is $\alpha_b = -0.9$. In order to determine the spectral index of c we compared its flux density seen at 22 GHz with the combined flux density of components c2 and c3 at 43 GHz. For c we thus obtain $\alpha_c = -1.4$. We find that the spectral index of component b is flattening with time ($\alpha_b = -1.60$ at epoch 1990.48 (Alberdi et al. 1993b) and $\alpha_b = -0.9$ at epoch 1992.5). The brightening, deceleration and spectral flattening of component b can be explained by motion of component b on a bent trajectory curving *towards* the observer. The observed changes are then due to differential changes of the Doppler-boosting factor with time.

(iii) Inspection of the spectral index map (Fig. 5) shows two dominant effects: in the regions associated with d, b and a, a spectral index gradient parallel to the mean jet axis (the ridge line of the jet) is found, and the spectrum steepens with increasing separation from d. However, in the region associated with c (the bridge), the spectral index flattens towards the northern edge of the jet. The spectral index gradient therefore is oriented tranverse to the jet axis, and reflects the difference in morphology of the jet at the two frequencies: in the regions between components b and d, the 43 GHz structure seems to be more strongly bent than the 22 GHz structure (this bending is consistently seen in maps and modelfits, see Fig. 2 & 3, and Table 4). This bending is also seen from the differences of the position angle of components c2 and c3 (relative to b), which are as large as 5-10 degrees between both frequencies (see Table 4). Independent evidence for the reality of this effect comes from maps obtained at lower frequencies and other epochs. The comparison of the structures seen at 22 GHz and 8.4 GHz (Alberdi et al. 1993a) similarly show enhanced jet curvature at the higher frequency. It is therefore clear that the projected spatial location of the peak of emission in 'the bridge' between component b and d changes systematically with frequency between 8.4 and 43.2 GHz.

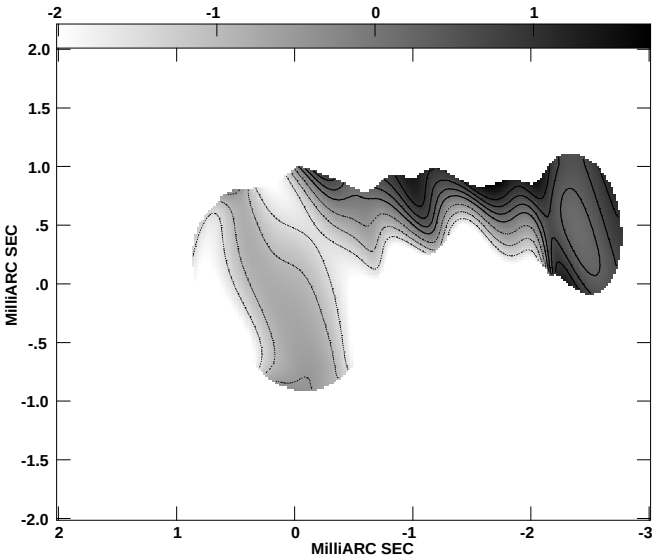

Fig. 5. Spectral index VLBI image of 4C 39.25 between 7 mm and 1.3 cm. The contour levels are -90, -60, -30, 0, 20, 40, 60% of the brightness spectral index map peak of 1.65. See Text.

4.5. Interpretation

Curvatures in parsec-scale radio jets seem to be quite common in extragalactic flat spectrum radio sources. The VLBI monitoring of e.g. 3C 345 (e.g. Biretta et al. 1986; Zensus 1991), 3C 273 (e.g. Zensus et al. 1988, 1990, Krichbaum et al., 1990 & 1993d), 3C 84 (e.g. Krichbaum et al. 1992, Venturi et al. 1993), 1803+784 (Krichbaum et al. 1993c & 1994), OJ 287 (Krichbaum et al. 1993d & 1994, Tateyama et al., 1996) reveals jet curvatures on sub-mas scales and evidence for motion along bent trajectories on sub-mas to mas-scales. Moreover, recent work on 3C 345 shows that the inner jet components move on differently curved paths (Zensus et al. 1995) indicative for motion in a helical conical jet (Steffen et al., 1995).

Our data enable us to get an estimate of the physical conditions within the source. We can determine the magnetic field strength within the individual components from synchrotron self-Compton calculations (Kellermann & Pauliny-Toth (1969) and Marscher (1980)) which is independent of the luminosity distance of the source. However, we can give only upper limits to B_{sync}/δ since i) the angular diameter of the components is only an upper limit (the components are unresolved at the ob-

serving frequency), ii) the turnover frequency of the individual components is not properly sampled and iii) we assume for the spectral index the determined value of α_{thin}. With these restrictions and taken into account of the values given in Table 4, we obtain the following upper limits for the individual magnetic fields: $B_a < 134\delta$ mG, $B_b < 50\delta$ mG, $B_d < 133\delta$ mG.

Three-dimensional jet bending seems to be present in 4C 39.25. The coexistence of superluminal and stationary jet components, the apparent deceleration and simultaneous brightening of b and its spectral flattening are consistently explained in a helically twisted jet geometry (see Sects. 3 and 4).

At present, the physical reason for jet bending is not well understood. The observed non-ballistic motion along curved trajectories excludes orbital precession as the main cause for such bending. Helical features in jets might be explained by three-dimensional hydrodynamical Kelvin-Helmholtz instabilities (eg. Hardee et al. 1990, 1995) or by helical magnetic fields in magneto-hydrodynamical jet scenarios (e.g. Blandford and Payne, 1982; Königl and Choudhuri, 1985; Camenzind 1986, 1989; Uchida et al. 1990). Following these ideas, motion along curved paths could result from motion along helical twists in the jet. In such models, patterns moving with different speeds than that of the underlying bulk jet flow and filamentary jet structures are also possible. These filaments or oblique features must not necessarily fill the full jet-width, but could fill only part of it. This could explain many of the observed properties of the sub-milliarcsecond relativistic jets. Families of cylindrically nested magnetic surfaces and/or flux tubes, which guide the plasma could be expected in jets dominated by strong magnetic fields (eg. Camenzind 1990). In similar models to the 'nested magnetic flux tubes' like the two-fluid model (Sol et al. 1989, Pelletier & Roland, 1990), transverse gradients of plasma density and velocity could be expected.

Observational evidence for spectral index gradients, for the transverse jet structures and for the fact that jet components might not completely fill the full width of the jet comes from VLBI observations of a number of objects eg. 3C 345, in which all jet components – albeit moving on different trajectories – are located within a larger parabolically bent jet envelope (Zensus et al. , 1995). In 0735+178 (Gabuzda et al. 1994) and 1803+784 (Krichbaum et al. 1993c, Britzen & Krichbaum, 1995) a moving component passed a stationary feature with no evidence for interaction between both components. This suggests distinct spatial component locations, and component sizes not completely filling the full transverse width of the jet. Edge- and limb-brightening of jets are observed, for example, in M 87 (Biretta et al. 1989), in 3C 273 (Unwin et al. 1994), and in polarized light also in the S5-quasar 0836+710 (T. Cawthorne, *priv. communication*). In edge- or limb-brightened jets, opacity changes along the transverse jet-width could be expected, although these effects are not yet well investigated in detail.

The observed frequency dependent jet morphology of 4C 39.25, the apparent differences of the jet curvature in the 'bridge' of emission near component c, and the transverse spectral index gradient in this region are indicative for internal transverse jet structures and oscillations on pc- to sub-pc scales in this source. A quantitative modelling of the detailed jet physics requires, for example, knowledge of the transverse velocity-, density-, and magnetic field distribution and of the jet geometry. All this could be observationally determined from this and future multifrequency high angular resolution VLBI-monitoring experiments (preferably with total intensity and polarization).

5. Conclusions

We observed the parsec scale radio jet of the compact radio source 4C 39.25 with VLBI at millimeter wavelengths (λ3 mm, λ7 mm and λ1.3 cm). The jet with its components a, b and c shows steep spectra characteristic of optically thin synchrotron emission. The spectrum of the westernmost unresolved component d peaks between 43 and 86 GHz, supporting its identification as the self-absorbed true core of 4C 39.25. The morphology of a 'bridge' of emission, connecting b and d is more complex than previously thought and apparently different at 22 and 43 GHz, showing a more pronounced bending towards the north at the higher frequency. A spectral index map of 4C 39.25 made from quasi-simultaneously obtained 22 and 43 GHz VLBI images shows that the region of the jet associated with component d has an inverted spectrum and that a and b have steep spectra. In these components, the spectral index steepens *along* the jet (the spectral index gradient is parallel to the mean jet axis). In contrast to it, the spectral index gradient in the region associated with the 'bridge of emission' (component c) is transverse (perpendicular) to the mean ridge line of the jet. We interpret the frequency dependent jet structure and curvature as being due to opacity effects in a bent relativistic jet and argue that models which use helical Kelvin-Helmholtz instabilities and/or special (e.g. helical) magnetic field configurations could – at least in principle – explain the observed behaviour.

Acknowledgements. We would like to thank the many people who made these observations possible. In particular, we want to thank Dr. Ralf Wegner, Dr. Wolfgang Steffen and Silke Britzen from MPIfR for help during the observations. We express special thanks to Dr. W. Alef for his help during the correlation and fringe fitting, and to the operators U. Stursberg, and H. Blaschke for their work at the MK III-correlator of the MPIfR. Thanks are also due to the staff of the radio-observatories for their efforts. Thanks also to the referee, Dr. D. Fraix-Burnet, for his suggestions to improve the paper. This research has been supported in part by the Spanish DGICYT research grants PB 93-0030 and PB 94-1275, and the research grant from the Junta de Andalucia. The work of TPK was supported by the German BMFT-Verbundforschung. The National Radio Astronomy Observatory is operated by Associated Universities Inc., under cooperative agreement with the National Science Foundation. The work at Haystack is also in part supported by the NSF. Onsala Space Observatory is the Swedisch National facility for Radio Astronomy.

References

Alberdi, A., Marcaide, J.M., Marscher, A.P., Zhang, Y.F. et al. 1993a, ApJ, 402, 160.

Alberdi, A., Krichbaum, T.P., Marcaide, J.M., Witzel, A. et al. 1993b, A&A, 271, 93.

Alberdi, A., Gómez, J.L., Marcaide, J.M. 1993c, in: Sub Arcsecond Radio Astronomy, ed. R. Davis and R.S. Booth (Cambridge University Press), p. 355.
Alef, W., and Porcas, R.W. 1986, A&A, 168, 365.
Bartel, N., Dhawan, V., Krichbaum, T.P., Graham, D.A. et al. 1988, Nat, 334, 131.
Biretta, J.A., Moore, R.L., Cohen, M.H. 1986, ApJ, 308, 93.
Biretta, J.A., Owen, F.N., Cornwell, T.J. 1989, ApJ, 342, 128.
Blandford, R.D. & Königl, A. 1979, ApJ, 232, 343.
Blandford, R.D. & Payne, D.G., 1982, MNRAS, 199, 883.
Britzen, S., and Krichbaum, T.P., 1996, in: Proceedings of the 10th Working meeting on European VLBI for Geodesy and Astronomy, eds. R. Lanotte and G. Bianco, Matera (Italy), in press.
Camenzind, M. 1986, A&A, 156, 137.
Camenzind, M. 1989, in: Accretion Disks and Magnetic Fields in Astrophysics, ed. G. Belvedere, Kluwer-Dordrecht, p. 129.
Camenzind, M. 1990, in: Reviews in Modern Astronomy: "Accretion and Winds", ed. G. Klare, Springer-Verlag, p. 234.
Clark, B.G. 1973, Proc. IEEE 168, 1242.
Cornwell, T.J., Wilkinson, P.N. 1981, MNRAS, 196, 1067.
Gabuzda, D.C., Wardle, J.F.C., Roberts, D.H., Aller, M.F., Aller, H.D. 1994, ApJ, 435, 128.
Gómez, J.L., Alberdi, A., Marcaide, J.M. 1993, A&A, 274, 55.
Gómez, J.L., Alberdi, A., Marcaide, J.M. 1994, A&A, 284, 51.
Guirado, J.C., Marcaide, J.M., Alberdi, A., Elósegui, P. et al. 1995, AJ, 110, 2586.
Hardee, P.E. 1990, in: Parsec-scale radio jets, ed. J. A. Zensus and T. J. Pearson (Cambridge University Press), p. 266.
Hardee, P.E., Clarke, D.A., Howell, D.A. 1995, ApJ, 441, 644.
Kellermann, K.I. & Pauliny-Toth, I. 1969, ApJ, 155, L71
Krichbaum, T.P., Booth, R.S., Kus, A.J. et al. 1990, A&A, 237, 3.
Krichbaum, T.P., Witzel, A., Graham, D.A. et al. 1992a, A&A, 260, 33.
Krichbaum, T.P., Witzel, A., Graham, D.A., Standke, K.J. et al. 1993a, A&A, 275, 375.
Krichbaum, T.P., Zensus, J.A., Witzel, A. et al. 1993b, A&A, 274, L37.
Krichbaum, T.P., Witzel, A., Graham, D.A., Schalinski, C.J., Zensus, J.A., 1993c, in: Sub Arcsecond Radio Astronomy, ed. R. Davis and R.S. Booth (Cambridge University Press), p. 181
Krichbaum, T.P., Witzel, A., Graham, D.A. 1993d, in: Jets in Extragalactic Radio Sources, ed. K. Meisenheimer et al. (Springer, Heidelberg), p. 71
Krichbaum, T.P., Witzel, A., Standke, K.J., Graham, D.A. et al. 1994, in: Compact Extragalactic Radio Sources, ed. J.A. Zensus and K.I. Kellermann (NRAO, AUI), p. 45.
Krichbaum, T.P., Standke, K., Witzel, A. et al. 1995, in: Proceedings of the 2nd EVN/JIVE Symposium, ed. A.J. Kus, R.T. Schilizzi, K.M. Borkowski and L.I. Gurvits (TRAO), p. 47.
Königl, A. & Choudhuri, A.R. 1985, ApJ, 289, 173.
Lobanov, A.P. 1995, Ph. D. Thesis
Marcaide, J.M. & Shapiro, I.I. 1983, AJ, 88, 1133.
Marcaide, J.M., Bartel, N., Gorenstein, M.V. et al. 1985, Nat, 314, 424.
Marcaide, J.M., Alberdi, A., Elósegui, P., Schalinski, C.J. et al. 1989, A&A, 211, L23.
Marcaide, J.M., Alberdi, A., Elósegui, P., Marscher, A.P. et al. 1990, in: Parsec-scale radio jets, ed. J. A. Zensus and T. J. Pearson (Cambridge University Press), p. 59.
Marcaide, J.M., Alberdi, A., Gómez, J.L., Guirado, J.C. et al. 1994, in: Compact Extragalactic Radio Sources, ed. J.A. Zensus and K.I. Kellermann (NRAO, AUI), p. 141.
Marscher, A.P. 1980, ApJ, 235, 386.
Marscher, A.P., Shaffer, D.B., Booth, R.S., Geldzahler, B.J., 1987, ApJ, 319, L69.
Marscher, A.P., Zhang, Y.F., Shaffer, D.B., Aller, H.D., Aller, M.F. 1991, ApJ, 371, 491.
Pearson, T.J. 1991, BAAS 23, 991.
Pearson, T.J., Shepherd, M.C., Taylor, G.B., Myers, S.T. 1994, BAAS 185, 808.
Pelletier, G., Roland, J. 1990, in: Parsec-scale radio jets, ed. J. A. Zensus and T. J. Pearson (Cambridge University Press), p. 323.
Rogers, A.E.E., Capallo, R.J., Hinteregger, H.F. et al. 1983, Sci, 219, 51.
Shaffer, D.B., Marscher, A.P., Marcaide, J.M., Romney, J.D. 1987, ApJ, 314, L1.
Sol, H., Pelletier, G. & Asséo, E. 1989, MNRAS, 237, 411.
Standke, K., Krichbaum, T.P., Witzel, A., Graham, D., Schalinski, C.J. 1994, VLBI Technology, Progress and Future Observational Possibilities, ed. T. Sasao, S. Manabe, O. Kamaye and M. Inoue (Terra Scientific Publishing Company, Tokyo), p. 75.
Steffen, W., Zensus, J.A., Krichbaum, T.P., et al. 1995, A&A, 302, 335.
Tateyama, C.E., Inoue, M., Krichbaum, T.P., et al. 1996, PASJ, 48, 37.
Uchida et al. 1990, in: Galactic and Intergalactic Magnetic Fields, ed. R. Beck et al. (Kluwer, Dordrecht), p. 425.
Unwin, S.C., Davis, R.J., Muxlow, T.W.B. 1994, in: Compact Extragalactic Radio Sources, ed. J.A. Zensus and K.I. Kellermann (NRAO, AUI), p. 81.
Venturi, T., Readhead, A.C.S., Marr, J.M., and Backer, D., 1993, ApJ, 411, 552.
Zensus, J.A., Bååth, L.B., Cohen, M.H., Nicolson, G.D. 1988, Nat, 334, 410.
Zensus, J.A., Unwin, S.C., Cohen, M.H., Biretta, J.A. 1990, AJ, 100, 1777.
Zensus, J.A. 1991, in: Frontiers of VLBI, Frontiers Science Series No. 1, ed. H. Hirabayashi, M. Inoue and K. Kobayashi (Universal Academy Press, Tokyo), p. 321.
Zensus, J.A., Lobanov, A.P., Krichbaum, T.P. 1995, in Quasars and AGN: High Resolution Radio Imaging, ed. M. Cohen and K.I.K. Kellermann (Proc. Nat. Acad. Sci., USA), 92, 11348.
Zhang, Y.F., Marscher, A.P., Shaffer, D.B., Marcaide, J.M. et al. 1990, in: Parsec-scale radio jets, ed. J. A. Zensus and T. J. Pearson (Cambridge University Press), p. 66.

This article was processed by the author using Springer-Verlag LaTeX A&A style file *L-AA* version 3.